TRR
JOURNAL OF THE TRANSPORTATION RESEARCH BOARD

Research Article

Transportation Research Record
2022, Vol. 2676(1) 242–255

DOI: 10.1177/03611981211036685
journals.sagepub.com/home/trr
SAGE

Case Study of Drone Delivery Reliability for Time-Sensitive Medical Supplies With Stochastic Demand and Meteorological Conditions

Travis B. Glick[1], Miguel A. Figliozzi[1], and Avinash Unnikrishnan[1]

Abstract

Drones are increasingly being utilized to deliver medical supplies, and the COVID-19 pandemic has accelerated this trend. Drones arrive quickly by taking more direct paths and avoiding ground-based obstructions. However, drones are not completely reliable and may also experience failures and delays. For consumer products, delivery delays are an inconvenience, but for some medical supplies, delays may be fatal. This research focused on the drone reliability of one particular type of supply and event: automatic defibrillators for out-of-hospital cardiac arrests. A modeling framework was developed to analyze drone delivery reliability with stochastic demands and meteorological conditions. Using probability distributions based on real data from Portland, OR, this research quantified the failure rates as a function of drone range and meteorological conditions that included temperature, precipitation, and wind. Tradeoffs among drone reliability, fleet size, population size, and meteorological conditions were analyzed.

Drone deliveries are being tested across the globe to meet not only parcel delivery demands but also to open new service models and opportunities where traditional ground delivery methods are relatively slow and unreliable. The delivery of medical supplies is an area that has sparked high interest because such supplies are often subject to strict temporal constraints. For example, drones have already been employed for the delivery of medical supplies in Rwanda, a country that experiences heavy rains that often lead to road impassibility (*1*). Hospital supply chains in Rwanda now utilize drones for the delivery of blood from central storage facilities (*2*, *3*). Although blood deliveries are time-sensitive, some medical supplies are subject to even more stringent time considerations.

COVID-19 and the consequent lockdown have temporality removed some regulatory barriers for the deployment of drones. Drones are now being tested in several states such as Florida, North Carolina, North Dakota, and Virginia to deliver prescriptions, and there is a promising trial underway in Baltimore delivering kidneys for transplants (*4*). Even though there is the potential for a wide range of drone applications in the health sector, this research and case study focused on time-sensitive cardiac arrests.

Cardiac defibrillation (*5*) needs to be administered minutes after diagnosis to avoid patient death, but the majority (63%) of cardiac arrest cases occur outside of hospitals where defibrillators are not readily available. The survival rate for out-of-hospital cardiac arrest (OHCA) in 2016 was 12%, almost half that of the in-hospital rate (25%) (*6*). Currently, automatic external defibrillators (AED) weigh 1.1 kg (2.4 lb), take just 1.77 L (108 in.^{3}) of space, and come with instructions to guide nonmedical persons through the machine's use (*7*). This makes AEDs an ideal candidate for drone delivery. However, the seriousness of cardiac arrest puts tight constraints on adequate arrival times. Even in hospitals, defibrillation survival rates after 3 min are reduced from 39% to 22%, and each additional minute reduces the chance of survival by approximately 4% (*8*). Currently, the average ground-based (ambulance) emergency response time in the United States is much longer than 3 min, with a mean of 7.0, 7.7, and 14.5 min for urban,

[1]Department of Civil and Environmental Engineering, Portland State University, Portland, OR

Corresponding Author:
Miguel A. Figliozzi, figliozzi@pdx.edu

suburban, and rural areas, respectively (*9*). As drones are not subject to typical ground road infrastructure restrictions, they may have a higher probability of timely response.

Pilots for medical supply deliveries using drones have begun in the United States (*10*), and recent research into drone deliveries of AEDs has attempted to quantify delivery times, estimate mortality rates, and optimize delivery networks through theoretical models (*11–13*). These studies have provided useful tools for AED delivery but have ignored key factors such as weather. Such exclusions and the lack of real-world data mean the viability of drone deliveries for time-sensitive supplies remains an open question.

This research focused on drone deliveries of AEDs for OHCA and fills a gap in recent research by using real-world data to model and assess the impact of weather on drone delivery reliability and to quantify the impact of fleet size and population on failure rates. Determining the number of drones required to service an area is challenging as the rate of cardiac events for an area is dependent on population size and time of day (*5*).

The remainder of this paper is structured as follows: first, demand and estimate failure rates are modelled as a function of drone fleet size and population for two types of drone operations: battery recharging and battery swapping. Second, temperature, precipitation, and wind using historical data from Portland, OR are modelled. Third, the impact of temperature, precipitation, and wind on range and drone delivery failure are quantified. Finally, conclusions, based on the results, are discussed with recommendations for future studies.

Modeling Demand, Fleet Size, and Failure Rate

The American Heart Association (AHA) provides a population mean (μ_N) and confidence intervals (CIs) for the number of OHCA events in a year (*6*). From the CIs, a population variance (σ_N^2) can be calculated; μ_N and σ_N^2 are for the U.S. population as a whole (N), not for a selected sample of n people. For a sample population over 1 year, the mean and standard deviation for the number of OHCA can be calculated as

$$\mu_N = 356,461 \quad \sigma_N = 3,067$$
$$\mu_n = \left(\frac{n}{N}\right)\mu_N \quad \sigma_n = \sqrt{\left(\frac{n}{N}\right)\sigma_N^2}$$

Modeling the number of occurrences in a given time interval is a common application of the Poisson distribution with parameter λ_n. To capture the variation of λ_n for a given population, λ_n is also simulated using a gamma distribution with shape and rate parameters α and β, respectively. In Bayesian statistics, the gamma distribution is the conjugate prior for Poisson, and equations for the mean and variance can be defined as follows (*14*):

$$E[\lambda_n] = \mu_n = \frac{\alpha}{\beta} \quad Var[\lambda_n] = \sigma_n^2 = \frac{\alpha}{\beta^2}$$

Solving for α and β, the parameters of the gamma distribution for λ_n are,

$$\alpha = \frac{\mu_n^2}{\sigma_n^2} = \frac{\left(\left(\frac{n}{N}\right)\mu_N\right)^2}{\left(\frac{n}{N}\right)\sigma_N^2} = \left(\frac{n}{N}\right)\frac{\mu_N^2}{\sigma_N^2} \quad \beta = \frac{\mu_n}{\sigma_n^2} = \frac{\left(\frac{n}{N}\right)\mu_N}{\left(\frac{n}{N}\right)\sigma_N^2} = \frac{\mu_N}{\sigma_N^2}$$

For any population, n, the number of cardiac events in a year can be simulated using

$$\lambda_n \sim Gamma\left(\alpha = \left(\frac{n}{N}\right)\frac{\mu_N^2}{\sigma_N^2}, \beta = \frac{\mu_N}{\sigma_N^2}\right)$$

Given this formulation, random OHCA events were simulated using a Poisson distribution with rate parameter λ_n, defined by AHA data. The above equations provide estimates for a full year. However, the number of OHCA is also temporally dependent.

There was no statistically significant variation across months or seasons, but day-of-the-week and time-of-day did have significant variation. Incidence rate ratios (IRRs) with 95% CIs were used for simulation, where the highest increases were seen on Mondays (1.18, 1.38) and during the 8:00 to 9:00 a.m. hour (1.96, 2.59) (*15*). Combined, Monday mornings had an average rate increase of 2.91 over the yearly average OHCA rate. Normal distributions were assumed for each IRR, based on the central limit theorem of probability (*14*), and the time between consecutive OHCA events were simulated utilizing a Poisson process of rate λ_n. Figure 1 shows the asymmetry of the distribution around the mean for the time between events as a function of population size.

Fleet Size, Drone Repositioning, and Battery Swapping Times

The number of required drones was based on the shortest time between events, given the nearly three-times increase over the average rates for Monday mornings, but also on the time it takes to serve a patient and reposition a drone. The calculated number of drones, therefore, was the minimum required during peak demand and above the minimum for all other days of the week and times of day. Two options were considered: in-drone battery recharging and battery swapping. For this study, we assumed that a high-performance multicopter MD4-3000 drone was utilized. Drone specifications are given in Table 1 (*16*).

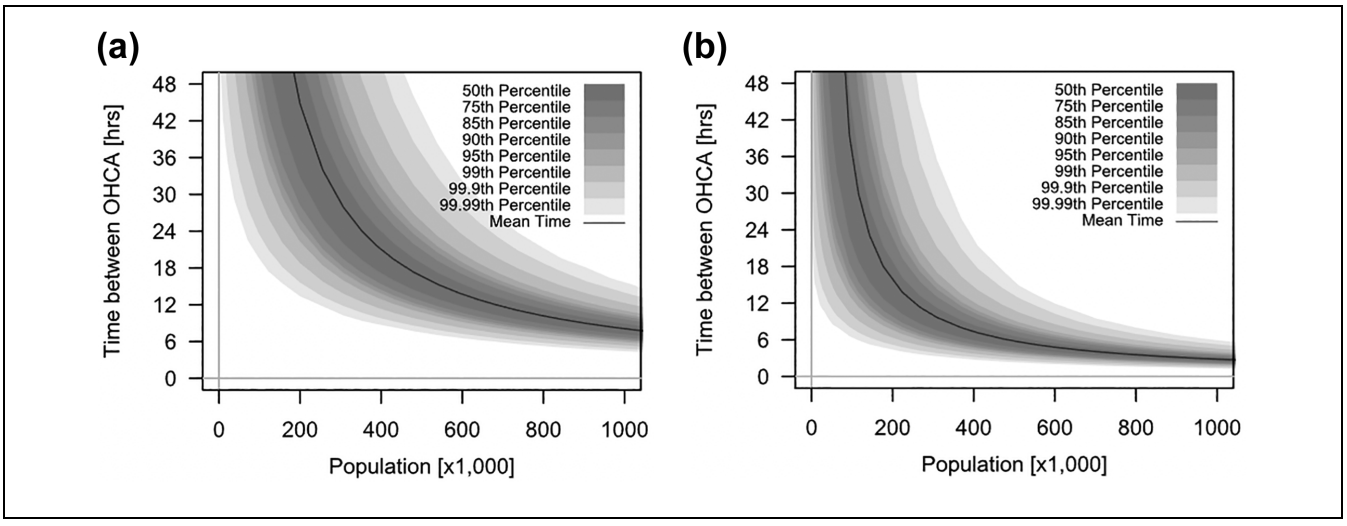

Figure 1. Time between consecutive out-of-hospital cardiac arrest (OHCA) events versus population for (*a*) U.S. average demand rate and (*b*) rate on Monday between 8:00 and 9:00 a.m.

Table 1. MD4-3000 Drone Characteristics

Specification	MD4-3000
Takeoff/gross weight, m	11.1 kg (24.5 lb)
Tare/curb weight, m_t	10.0 kg (22.1 lb)
Payload, m_l	1.1 kg (2.4 lb)
Empty weight factor, c_m	0.90
Battery/fuel storage capacity*	777 wh
Loaded flight time (m_l = 1.1 kg)	42 min
Range (m_l = 1.1 kg)	50 km (31 mi)

Note: * wh = watt-hour, from source (17)

The optimal range was assumed to be 50 km (31 mi), which assumes ideal weather conditions and a cruise speed of 20 m/s (44.7 mph). With a 1.1 kg (2.4 lb) payload, the flight time will be approximately 42 min. The battery capacity of drones used in this study had a 21,000 mAh (*17*). The LiPo battery has a recommended recharge rate of 2A at greater than 90% charge efficiency (*18*). Therefore, the charge time following a complete drain of the battery for one of these drones is between 10 h 30 min and 11 h 40 min. However, batteries will not experience a full drain each time they are used, and there will be additional variability in the charge times based on distance traveled.

Given the random distribution of OHCA events and the combination of service and charge time of batteries, M/M/c queuing theory can be employed to determine the number of drones required. For service times, it was assumed that a drone must stay with a patient until the paramedics arrive (an average of 8 min) (*9*), stabilize the patient (averaging 2 min), have the automatic defibrillator repackaged for the return trip (averaging 5 min), and return to base (averaging 5 min of flight and landing time). In addition to these 20 min of service time, drones are additionally unavailable to service new patients while their batteries are being recharged (Case 1) or swapped for a fully charged battery (Case 2).

In Case 1, given an average of 10 min active flight time to and from a patient and an available flight time of 42 min, the average recharge time would be about 2 h 40 min. Adding the 20 min of service time, the average usage time was 3 h, which corresponds to an average of eight possible services per day. Using an M/M/c queuing model, failure was defined as the probability that there would be one or more people in the queue (i.e., a person is waiting to be served owing to drone unavailability). The rate of OHCA (λ_n) used was the worst-case scenario (i.e., 8:00 to 9:00 a.m. on Mondays). Figure 2 shows the failure probability (plotted logarithmically) for Case 1, as a function of population and the number of available drones.

In Case 2, after 20 min of average service time, each drone was assumed to be unavailable for an additional 10 min (30 min total) to allow for the battery to be swapped with a fully charged battery. Figure 3 gives the failure probabilities for Case 2 given M/M/c queuing theory using the Monday morning rate. By swapping batteries, the number of possible services per day increased by a factor of 6, from 8 (in Case 1, battery recharging) to 48 (in Case 2, battery swapping).

For 100,000 people on Monday mornings, a single drone would fail to provide service 10.9% of the time in Case 1 versus just 1.8% of the time in Case 2. Picking an acceptable failure rate for vital medical supplies of $<0.1\%$, three drones would be required in Case 1, and two drones in Case 2. For 300,000 people and a $<0.01\%$

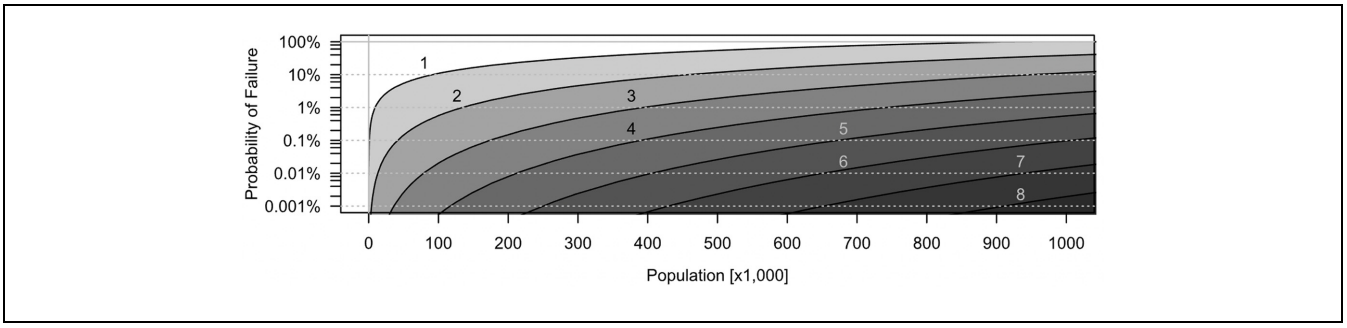

Figure 2. Case 1 (battery recharging): probability of failure versus population and number of drones given the demand rate on Mondays between 8:00 and 9:00 a.m.

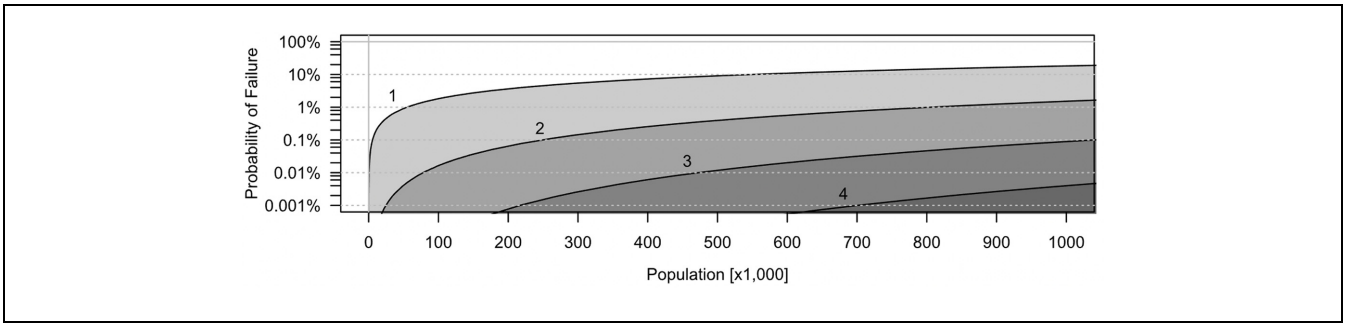

Figure 3. Case 2 (battery swapping): probability of failure versus population and number of drones given the demand rate on Mondays between 8:00 and 9:00 a.m.

failure rate, it would be five and three drones for Cases 1 and 2, respectively. This difference corresponds to notable cost savings; each drone can cost between $50,000 and $100,000 (*19*), but batteries cost between $300 and 600 (*18*). For 300,000 people and a failure rate of $<0.01\%$, consider a theoretical requirement of one extra drone in both cases, and one or 10 spare batteries per drone in Cases 1 and 2, respectively. Equipment costs would be 30% less in Case 2. Lastly, other extreme conditions, such as those caused by wildfires, are potential issues, but were outside the scope of the paper given the lack of detailed long-term wildfire data, the unique complexity of this topic, and the unusual set of operating constraints. A further potential issue is maintenance time and the mechanical reliability of drones, but this topic was also outside of the scope of this paper owing to the lack of drone reliability data.

Weather Modeling

Modeling Temperature Data and Distributions

Historical temperature data for a region typically gives a mean, high, and low temperature for each daily record. Figure 4 shows a histogram of January and July daily high temperatures from historical tables from Portland, OR. Given the shape of the temperature histograms, each month's high and low temperatures were assumed to follow a normal distribution. Therefore, historical data provide the ability to calculate means for high and low temperatures and their respective standard deviations for simulation. However, on a given day, high and low temperatures are highly correlated, and this must be considered for simulations.

To generate a pair of correlated random normal variables, y_1 and y_2, with known means, μ_1 and μ_2, variances, σ_1^2 and σ_2^2, and correlation, ρ, the following equation can be used (*20*):

$$\begin{array}{ll} x_1 = \mathcal{N}(0,1) & y_1 = \mu_1 + x_1\sigma_1 \\ x_2 = \mathcal{N}(0,1) & y_2 = \mu_2 + \sigma_2\left(x_1\rho + x_2\sqrt{1-\rho^2}\right) \end{array}$$

where y_1 and y_2 are the simulated low and high temperatures for a given day and will have the desired means, variances, and correlations. However, it is still possible for the high and low temperature to be reversed (i.e., $y_1 > y_2$). Simply swapping the values, such that all smaller values of the pair are in one list and larger values are in the other, will increase the correlation. Through simulation, this increase in correlation can be measured, and the ratio of the simulated correlation (ρ_s) and actual

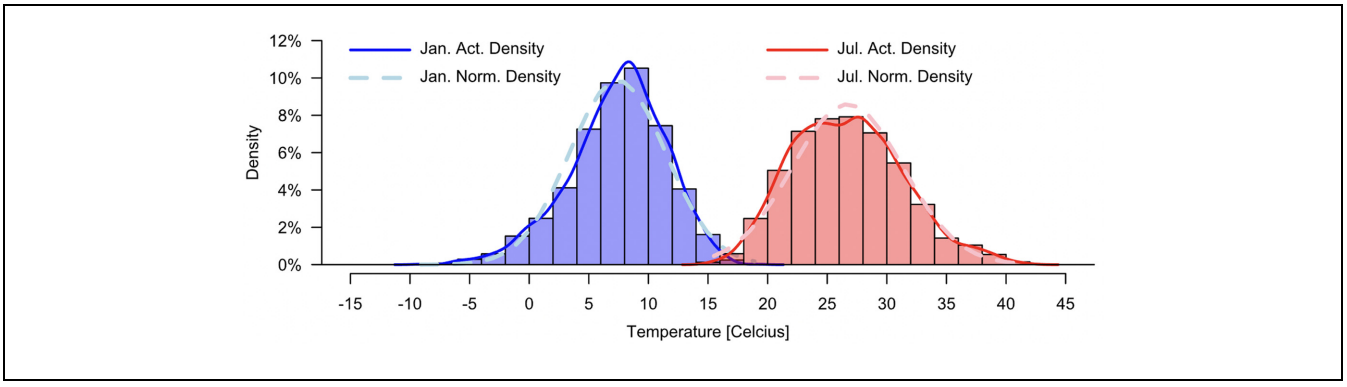

Figure 4. Histogram, density, and normal approximation of historical high temperatures for January and July.

Table 2. Historical Monthly High and Low Temperatures (°C) and Correlation Factors

	High temperature		Low temperature		Correlation	
Month	Mean	SD	Mean	SD	Observed	Corrected
January	7.41	4.04	1.19	4.12	0.788	0.782
February	10.34	3.61	2.31	3.52	0.534	0.523
March	13.08	3.76	3.70	2.98	0.243	0.225
April	16.09	4.36	5.64	2.77	0.285	0.271
May	19.80	4.99	8.76	2.70	0.390	0.377
June	22.82	4.82	11.68	2.31	0.418	0.409
July	26.70	4.64	13.84	2.11	0.422	0.420
August	26.69	4.53	13.95	2.21	0.286	0.282
September	23.92	4.79	11.26	2.82	0.169	0.158
October	17.61	4.10	7.59	3.23	0.286	0.269
November	11.40	3.50	4.25	3.84	0.639	0.629
December	7.80	3.65	1.90	3.77	0.775	0.769

Note: SD = standard deviation.

correlation (ρ) can be used to correct for the artificial increase,

$$\rho' = \frac{\rho}{\left(\frac{\rho_s}{\rho}\right)} = \rho\left(\frac{\rho}{\rho_s}\right) = \frac{\rho^2}{\rho_s}$$

Using ρ' in place of ρ and swapping paired values, as described above, results in a paired list of high and low temperatures with correlation ρ. Monthly trends from Portland's historical data are shown in Table 2, with both the observed correlation from the data (ρ) and corrected correlation (ρ') used for simulation. Unfortunately, these calculated means would be low if used for future predictions. Within the data set used in this analysis, there was a statistically significant positive slope for average high and average low temperatures of 0.01591 and 0.0228, respectively. For standard deviations, the slopes were statistically insignificant. Equations for the increase in mean highs and lows, compared with the aggregated historical averages, are given in the following, where y is the current year:

$$\Delta_{t_{lo}} = 0.0228y - 45.1480 \quad \Delta_{t_{hi}} = 0.0159y - 31.4535$$

The probability that the average daily and 8:00 a.m. temperatures are less than 0°C is important to the calculations of precipitation; as such, the increases are also important for future predictions. For any normally distributed variable, X, multiplied by a constant, c, the resulting distribution cX is also normal with mean, $c\mu$, and variance, $c^2\sigma^2$ (*21*),

$$X \sim \mathcal{N}(\mu, \sigma^2) \quad cX \sim \mathcal{N}(c\mu, c^2\sigma^2)$$

In addition, the sum of any two normally distributed variables, X and Y, with means, μ_1 and μ_2, variances, σ_1^2 and σ_2^2, and correlation, ρ, will also be normal (*22*),

$$X + Y \sim \mathcal{N}\left(\mu_1 + \mu_2, \sigma_1^2 + \sigma_2^2 + 2\rho\sigma_1\sigma_2\right)$$

Table 3. Probability of Zero Rain on a Given Day, and Daily Means and Variances of Precipitation for Each Month

Month	Probability of zero precipitation on a given day (%)	Daily precipitation rate (rate >0 mm)	
		Mean	Variance
January	32.6	7.7	77.1
February	36.6	6.4	59.2
March	35.3	5.6	35.5
April	42.0	4.2	21.7
May	54.0	4.7	30.1
June	64.6	4.4	28.8
July	86.6	3.7	22.8
August	83.8	4.6	34.7
September	72.8	5.6	55.9
October	52.7	6.5	61.6
November	32.7	7.7	83.2
December	31.4	8.0	81.9

For average daily temperature, the distribution of average temperature can be found by averaging the distributions of high and low temperatures. Given means, μ_1 and μ_2, variances, σ_1^2 and σ_2^2, and correlation, ρ, the distribution of the average daily temperature will be

$$\mathcal{N}\left(\frac{\mu_1}{2}+\frac{\mu_2}{2},\frac{\sigma_1^2}{2^2}+\frac{\sigma_2^2}{2^2}+2\rho\left(\frac{\sigma_1}{2}\right)\left(\frac{\sigma_2}{2}\right)\right)=\mathcal{N}\left(\frac{\mu_1+\mu_2}{2},\frac{\sigma_1^2+\sigma_2^2}{2^2}+\frac{\rho\sigma_1\sigma_2}{2}\right)$$

The probability that the average daily temperature is less than 0°C can be directly calculated for this normal distribution. This section presents the general statistical framework to analyze temperature. In the specific application and case study, at 8:00 a.m. (worst-case scenario), the probability was based only on the distribution of low temperatures.

Modeling Precipitation (Rain and Snow) Data and Distributions

Many regions have systems to measure rainfall. Often, the amount of rain per day and the amount of snow per day are included. For precipitation generally in the United States, 13 in. (33 cm) of snow equals 1 in. (2.54 cm) of precipitation. This conversion allows for total precipitation per day to be calculated. The same weather data set for Portland, OR, provided historical rain and snow measurements, which were combined. Table 3 shows the estimates for the mean and variance of precipitation on days with rainfall, and the calculated percent of days without rainfall for each month.

As with temperature, precipitation can be aggregated by month to account for monthly variation and subdivided into two distributions: Bernoulli probability of precipitation versus no precipitation, and a gamma distribution for the quantity of rain, given some rainfall (*23*). Given the daily average, μ, and daily variation, σ^2, of rainfall, the gamma parameters, α and β, can be calculated directly,

$$\alpha=\frac{\mu^2}{\sigma^2}\quad \beta=\frac{\mu}{\sigma^2}$$

A scalar constant applied to a gamma distribution is still gamma (*24*). For an hourly distribution, α would remain the same, but the rate parameter, β, would be multiplied by 24. To separate precipitation into rainfall and snow, the current temperature is needed. The correlated pair of high and low temperatures for the study period were used in combination with the mean correction factor.

For example, there was a 9.2% probability that the average daily temperature in January 2020 would be less than 0°C and a 32.6% probability of no rain. As such, the probability of snow was 6.2%, which corresponds to an average of 1.9 snowy days in January. However, during 8:00 a.m., there was a 30.5% probability temperatures would be below 0°C in 2020. Given the same probability of some rain, there was a 20.6% probability of snow during that hour, which corresponds to 6.4 mornings with some snow.

Modeling Wind Data and Distributions

A key factor that influences aviation performance is wind, and drones are highly susceptible because of their limited power and weight. The distribution of wind speeds can be modeled using a variety of known probability distributions with the Weibull ranking being among the best (*25*); however, several models have been shown to be adequate. The creation of wind models is dependent on both the amount of historical data and the

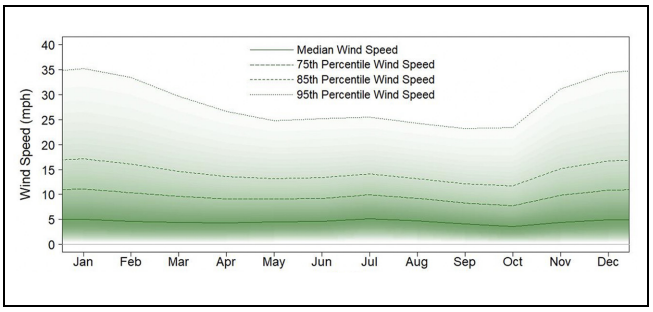

Figure 5. Simulated mean and confidence interval of wind speed in Portland, OR.

temporal granularity. For example, the inclusion of only a daily mean will not be sufficient to define most parametric models. However, a generalized understanding of wind effects does not require the accuracy of several climate models. As such, the choice of a probability distribution should be based on what can provide a reasonable approximation based on the available data (*26*).

There are long time series for Portland wind data, including historical average speeds, maximum gusts, percent calm, and direction. Gradient descent optimization was employed to find distribution parameters that provided reasonable approximations of historical trends. In Portland, different times of the year have different distributions of wind, which will directly influence failure odds. The distribution of wind speeds over a year is given in Figure 5.

Wind direction is also important. In Portland, winds mostly blow in the east-southeast direction during the winter months and the northwest direction during the summer months (see Figure 6). This factor is important for determining a drone's range at different times of the year. In January, areas to the northwest of a depot will be restricted by a headwind, whereas the opposite is true in July.

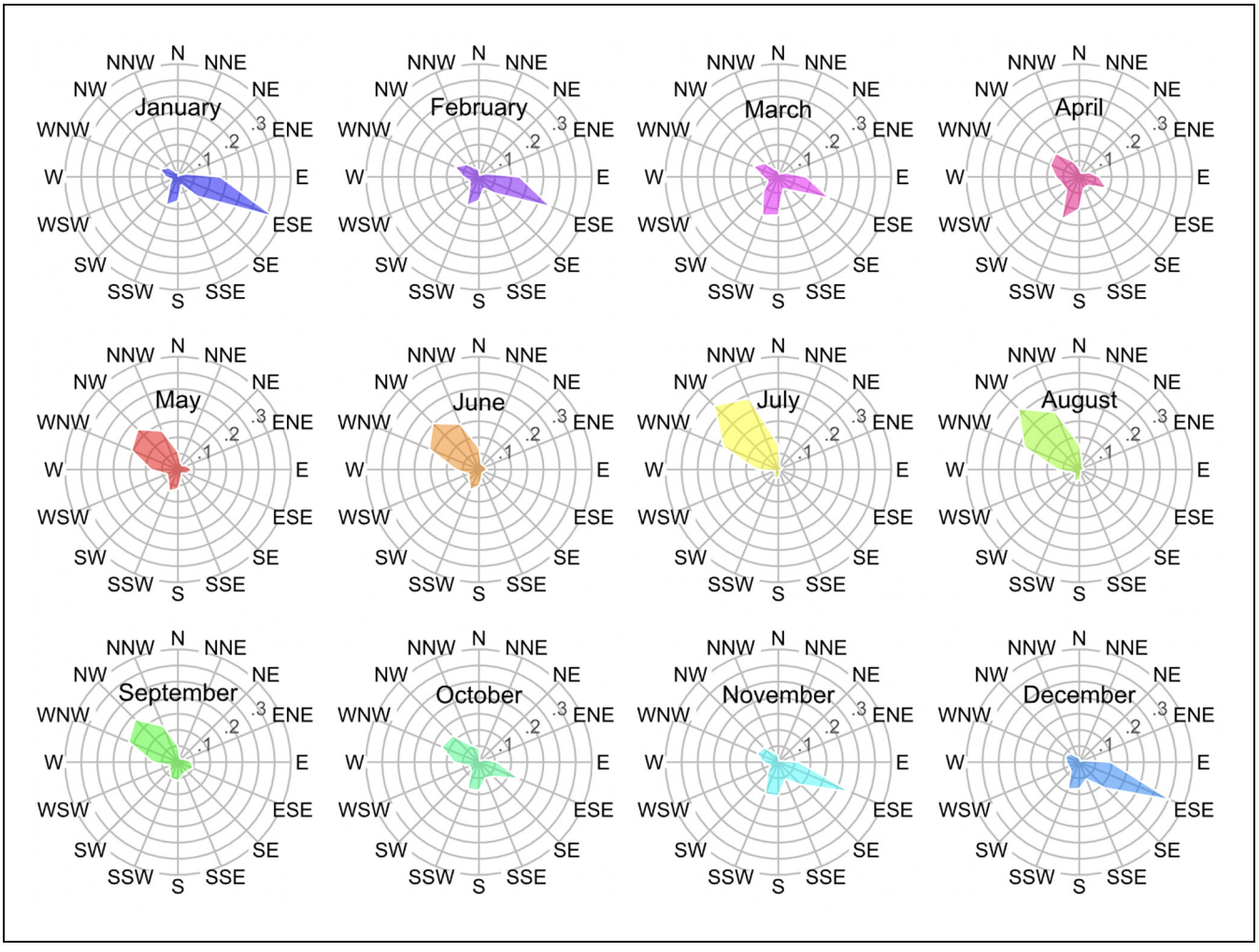

Figure 6. Probability of wind direction for each month in Portland, OR.

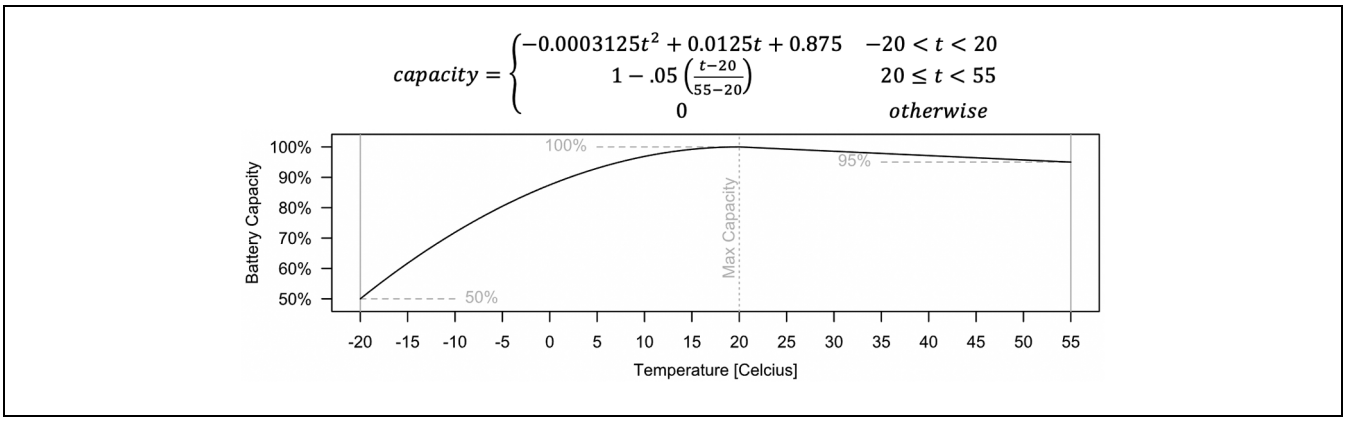

Figure 7. Battery capacity versus temperature and equations.

Range Reliability Modeling

The range of a drone is determined by its weight, flying efficiency, and battery capacity. For applications with a central hub, this range is half the distance a drone can travel, as a return trip must be accommodated. The following gives the energy necessary for level flight (*16*):

$$p_l(t) = \frac{(m_t + m_b + m_l)g}{\vartheta(s)\eta_p} d\,[\text{unitless} < 1] \qquad (1)$$

where

p_l = powerrequiredforlevelflight (watts),
t = traveltime (s) = (d/s),
m_b = dronebatterymass(kg),
m_l = droneload(defibrillator)mass(kg),
m_t = dronemasstare(i.e., withoutbatteryandload)(kg),
d = traveldistance (m),
$\vartheta(s)$ = lift − to − dragratio, or(L/D)(unitless),
s = travelspeed (m), and
η_p = totaldronepowertransferefficiency.

From Equation 1 it is possible to observe that energy consumption is directly proportional to drone mass and travel time and distance. The range estimations of this research considered the defibrillator 1.1 kg (2.4 lb) payload.

Modeling the Impact of Temperature

Temperature can have a significant impact on drone performance because drone lithium-ion batteries show optimal performance at approximately 20°C (68°F) but perform significantly worse at lower temperatures (see Figure 7). For lithium batteries, the output voltage is dependent on its operating temperature (*27*). In this study, battery available energy or capacity was assumed to decrease following a parabolic curve. The maximum (100%) will be at 20°C (68°F) and the minimum (50%) at −20°C (−4°F). At higher temperatures, the capacity decreases linearly from 100% to 95% from 20°C (68°F) to 55°C (131°F). Battery makers recommend no operation outside this temperature range (*18*).

In addition, battery capacity degrades linearly with the number of cycles up to a point. Often, the degradation accelerates when a battery reaches 80% of optimal capacity. At this point, the battery is considered unreliable and is no longer used. Before this point, the battery will have above 80% optimal capacity, but the exact amount will be unknown for any specific trip. As such, a random uniform distribution from 0.8 to 1.0 can be used in association with temperature for simulation to define the initial condition of the battery with an assumption that faulty or unreliable batteries will not be used.

OHCA events are more frequent during the 8:00 a.m. hour, which is typically the coldest hour of the day. As such, only the distribution of low temperatures is needed in this study. Figure 8 shows the means and CIs for daily high and low temperatures.

Figure 9 shows the probability of failure as a function of the total distance traveled, assuming an ideal 42-min flight time. The left and right edges of the shaded regions are defined using distributions of the low and high temperatures, respectively. The purple area is based on the yearly average highs and lows, whereas the blue region represents the worst-case (i.e., coldest) temperatures in January. The potential range of a drone will be half the total available flight distance, as return trips must be accommodated. The probability of failure is the percent of simulated trips that failed to reach a given range.

Winter will have the worst-case flight ranges as compared to the yearly averages. Yet, the range in the worst case was still larger than the maximum allowable in relation to time constraints for urgent medical deliveries. Even allowing for 14.5 min of flight time—the average ambulance arrival time in rural areas—more than 95% of drones would have enough charge for the 35-km (22-mi) trip, 17.5 km (11 mi) in each direction.

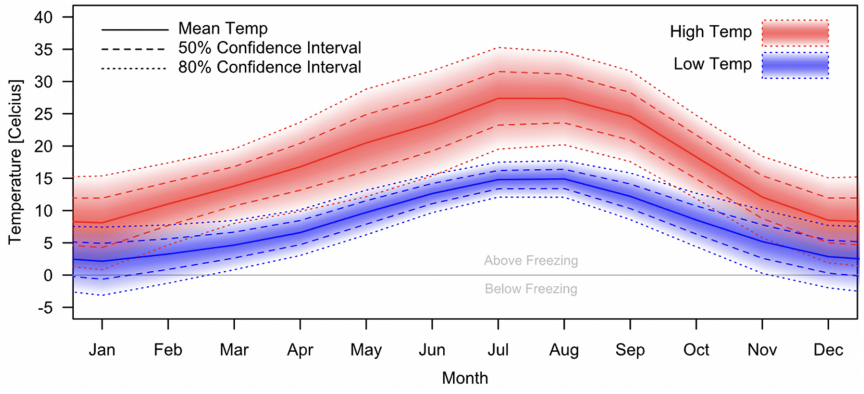

Figure 8. Means and confidence intervals for high and low temperatures by month.

In addition, the available range corresponded to a large service area. The 3-min delivery area covered 40 km^2 (15.7 mi^2), whereas 7 min (the urban ambulance average response time) allowed for an area of 222 km^2 (86 mi^2). This is functionally the size of many cities. Based on Portland weather conditions, large cities would require just a few drone hubs for full coverage.

Modeling the Impact of Precipitation

Several modern drones advertise some resistance to rain. As such, not all precipitation events would be considered failures. Considering rain alone (i.e., no snow), defining a specific cutoff for the permitted amount of rain would result in different failure odds. Figure 10 shows probability failure (plotted logarithmically) as a function of the maximum allowable precipitation rate. As an example, if drones are not sent during heavy rain, then drones will be unavailable (a failure condition) 4% of the time in January and $<0.1\%$ of the time in July.

Most drone manufacturers recommend not flying drones during snowfalls. As such, all snowy weather would cause a failure condition. However, if the amount of snow is considered such that some snowfall is acceptable, the failure rates would also be dependent on the precipitation cutoff (see Figure 11).

The cutoff points for snow and rain do not need to be equal. For example, if drones are permitted to fly in snow up to 10 mm/day (light snow) and rain up to 25 mm/day (light and moderate rain), then drones in January would be unavailable about 2% of the time because of snow and about 4% of the time owing to rain.

Modeling the Impact of Wind

For winds, the worst case is a headwind where the flight path is directly against the wind's direction of travel. In the best case, the drone has an increased speed resulting from a tailwind. Given a wind bearing, its speed, and a drone's flight speed, an angle-side-side triangle is formed (Figure 12). This arrangement requires an algorithm to solve as there might be 0, 1, or 2 possible answers. The following algorithm can be used to solve for the fastest feasible flight path, if possible. It combines the law of cosines and solves for the unknown using the quadratic formula.

Beginning with the law of cosines, where side A, side B, and angle β are known, but C is unknown, solve for 0, then put in the quadratic form with C as the unknown,

$$\begin{aligned} B^2 &= A^2 + C^2 - 2AC\cos(\beta) \\ 0 &= A^2 + C^2 - 2AC\cos(\beta) - B^2 \\ &= (1)C^2 + (-2A\cos(\beta))C + \left(A^2 - B^2\right) \end{aligned}$$

Solve for C using the quadratic formula and simplify,

$$\begin{aligned} C &= \frac{-(-2A\cos(\beta)) \pm \sqrt{(-2A\cos(\beta))^2 - 4(1)(A^2 - B^2)}}{2(1)} \\ &= \frac{2A\cos(\beta) \pm 2\sqrt{A^2\cos^2(\beta) - (A^2 - B^2)}}{2} \\ &= A\cos(\beta) \pm \sqrt{B^2 + A^2(\cos^2(\beta) - 1)} \\ &= A\cos(\beta) \pm \sqrt{B^2 - A^2\sin^2(\beta)} \end{aligned}$$

Mathematically, there are potentially two solutions, C_1 and C_2,

$$\begin{aligned} C_1 &= A\cos(\beta) + \sqrt{B^2 - A^2\sin^2(\beta)} \\ C_2 &= A\cos(\beta) - \sqrt{B^2 - A^2\sin^2(\beta)} \end{aligned}$$

However, in the context of flight speed triangles, negative and imaginary solutions are not applicable, and the fastest speed is preferred. Given that $C_1 \geqslant C_2$ for real

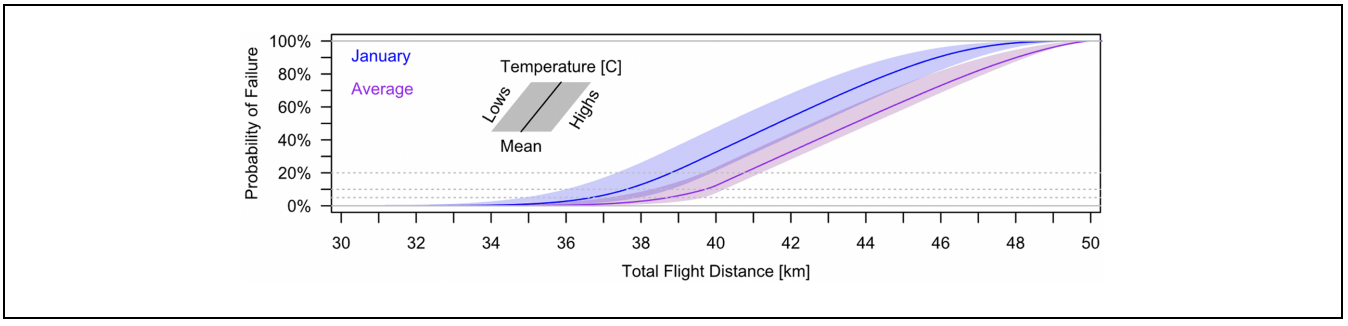

Figure 9. Probability of failure owing to temperature and available battery charge versus flight distance.

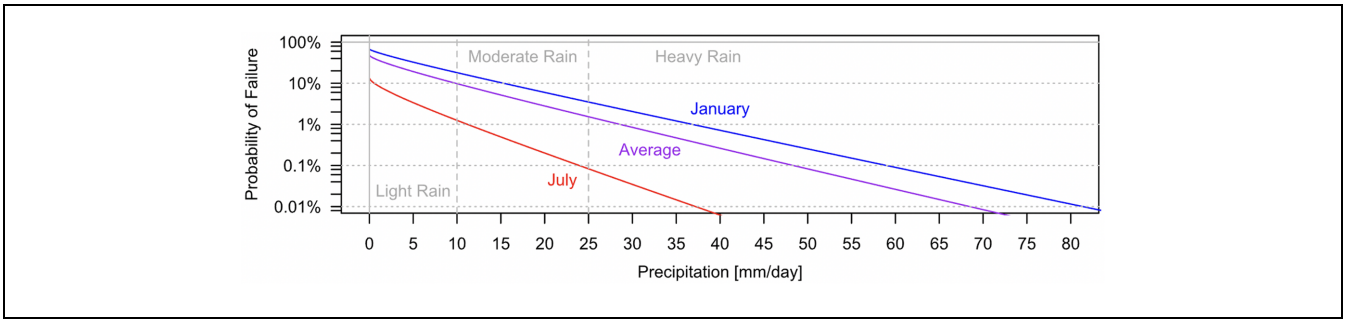

Figure 10. Probability of failure as a function of rainfall rate cutoff.

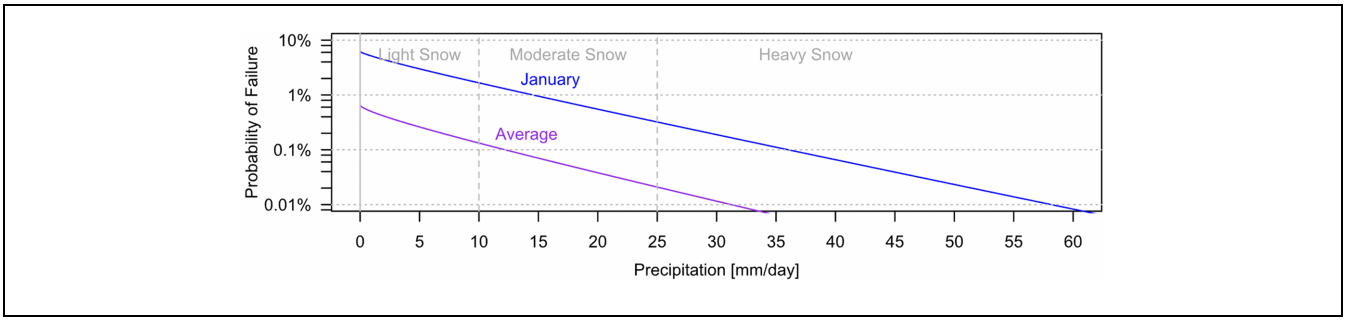

Figure 11. Probability of failure as a function of snowfall rate cutoff.

solutions, C_1 is used, given that the quantity under the square root is greater than 0.

As an example, assume a drone speed of 20 mps, wind speed of 30 mps, and a wind direction 30° away from the travel direction; both triangles in Figure 13 are valid solutions where the drone flies at a 20 mps and is able to reach the destination. The key factor is the effective travel speeds and initial flight bearings. A drone using the initial travel bearing from the second triangle would reach its destination three-times faster than a drone using the initial bearing from the first.

For headwind and tailwind simulations, flight times were held constant for arbitrarily selected 2-min and 10-min cases. For each trial, distance traveled within the

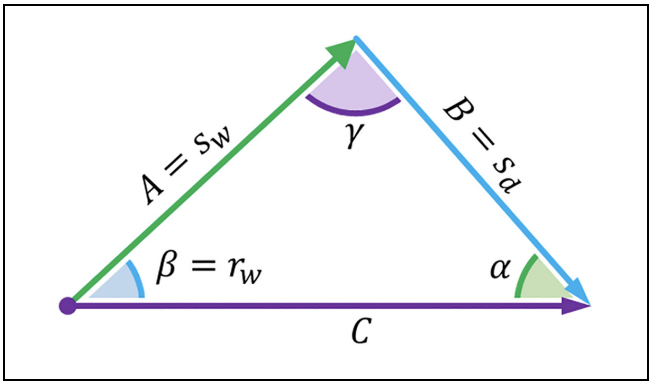

Figure 12. Setup and notation to solve an angle-side-side triangle, where s_w is wind speed, s_d is drone speed, and r_w is the angle between wind bearing and destination bearing.

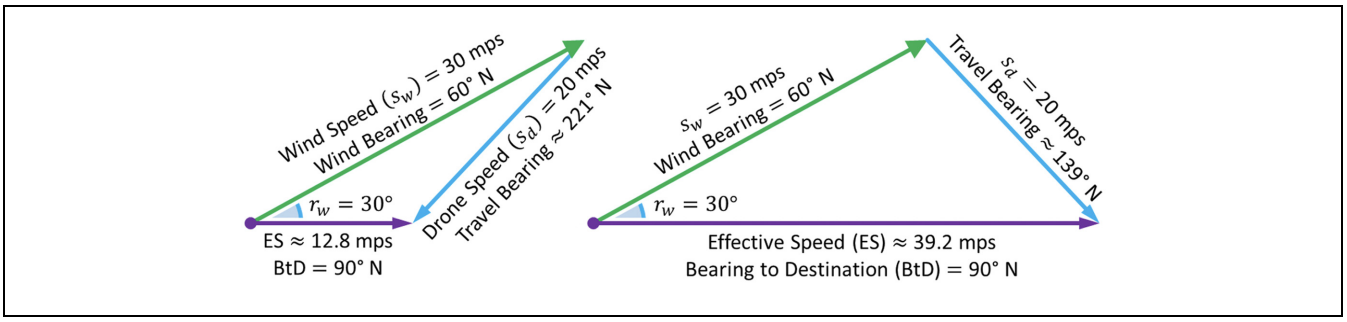

Figure 13. Two valid solutions to an angle-side-side triangle problem.

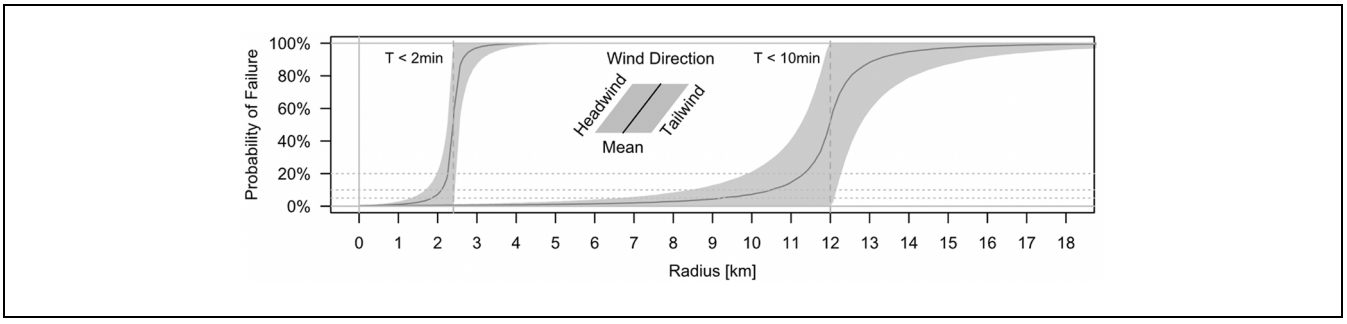

Figure 14. Probability of failure versus radius from wind with linear y-axis.

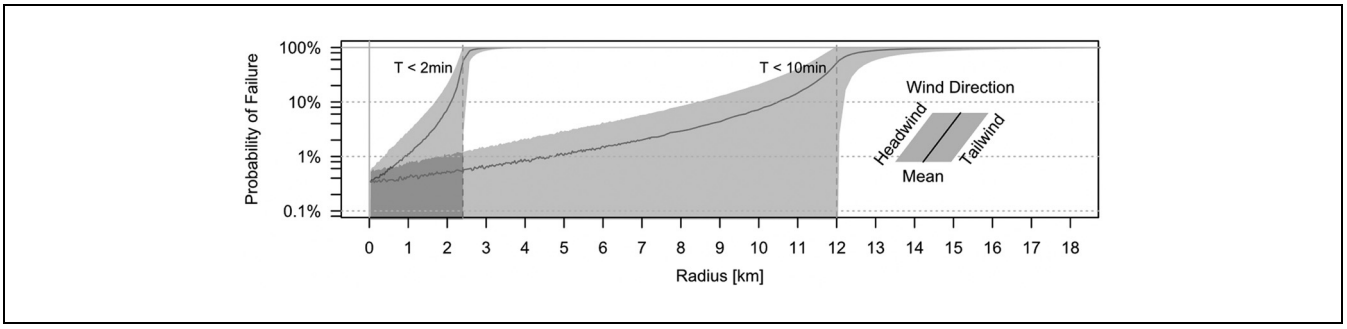

Figure 15. Probability of failure versus radius from wind with logarithmic y-axis.

time limit was recorded. The probability of delivery failures from wind was calculated based on the percent of trips that failed to reach a given distance within the allowable time. The shaded regions of Figures 14 and 15 show a range of failure probabilities between a simulated headwind versus a simulated tailwind and the result using a random bearing as the central line. As the flight time increased, the probability of failure also increased. In Figure 15, the y-axis of Figure 14 is transformed from linear to logarithmic.

At a 20% acceptable failure rate for 2-min deliveries, the worst case for the range decreased from 2.4 km (1.5 mi) to about 2 km (1.2 mi)—a reduction of 16%. At a 5% acceptable failure rate, the range further reduced to about 1.3 km (0.8 mi). Although the theoretical range of drones is large (see Figure 9), the practical range for timely deliveries is a limiting factor.

Figure 15 shows that the average potential failure from wind is above 0.1% for a 2-min or 10-min trip. Wind plays a key role in determining acceptable failure rates and for determining a potential range for drone deliveries. Notably, having multiple hubs would reduce failure rates from the wind as different hubs could be employed depending on wind direction. Headwinds and potential failure from one direction could be tailwinds and success from another.

Conclusions

For the delivery of time-sensitive supplies, drones might provide the means to bypass many obstacles experienced by ground transportation. However, drones are subject to their own set of constraints that limit the likelihood of successful deliveries. Although packages from an online retailer can be delayed by hours without substantial ill effect, even short delays in the context of medical supplies can be fatal. This research utilized real-world data to examine the impact of stochastic demand and weather conditions on drone delivery reliability.

The number of drones needed is highly dependent on charge times, use of battery swapping, and population in the service area. The specific application of drones to deliver defibrillators must consider that the average OHCA demand rate increases 2.91 times on a Monday morning. This worst-case scenario and economic considerations should be used to define the required equipment for a service area. Additional consideration should also be given to potential mechanical failures and maintenance schedules. Given the equipment costs, one potential solution is a requirement for one extra drone over the calculated minimum, extra batteries, and equipment to check battery health. Lastly, it is important to note that failure because of extreme weather conditions cannot be addressed by simply having more available drones. Extreme weather conditions that would result in a failed delivery for one drone, would result in a failed delivery for any other drone because drones cannot operate under extreme weather conditions. In summary, proper fleet sizing could address variability in demand as well as variability in weather conditions but will not eliminate delivery failures resulting from extreme weather conditions when drones cannot operate.

In this case study, wind was a key factor; even the average winds of Portland in January would cause failures, defined by travel time constraints more than 1% of the time. The direction of winds also changes depending on the time of year. The placement of drone hubs should consider ranges defined both by temporal constraints given by OHCA events survival rates as well as probabilistic failure odds caused by winds. Studies that examine multiple hubs could also consider potential failure rates and repositioning strategies considering the seasonality of weather conditions.

The temperature in Portland was not as crucial as wind in relation to reliable drone deliveries. The large potential delivery range of high-quality drones combined with strict delivery time limits reduced the negative effects of temperature and charge cycles. Therefore, temperature, as it relates to battery function, could be ignored for these types of deliveries since the potential for failure remained low. For example, a 14 km (8.7 mi) trip (28 km or 17.4 mi both ways) would have less than 0.001% failure odds owing to temperature and charge decay in the worst case. Although extreme temperatures have limited negative effects on batteries, wildfires, a cause of such extreme conditions, could potentially limit drone operations owing to difficult operating conditions and "no-fly orders" issued by federal, state, and local wildland fire management agencies and the Federal Aviation Administration (FAA) (*28*). Wildfires are an important issue, but outside of the scope of this paper owing to the lack of detailed historical data required to model and predict wildfire intensity, winds, location, and so forth. These issues are compounded by a dynamic problem from greenhouse gas emissions and their effect on wildfire characteristics and seasonality.

Precipitation failures are highly dependent on the level of precipitation considered too high to send a drone. The rate of failure, defined by the probability of not sending a drone, changes throughout the year and by time of day. If a drone is rated for higher water resistance, the failure rate will be lower. Furthermore, temperature is important as it relates to precipitation, as snow has larger adverse effects on drone operations compared with rain.

This paper has examined several of the mechanical and meteorological impacts on drone deliveries to examine which factors are most important and to define limits. The results indicated that successful drone deliveries of AEDs were highly influenced by wind speeds, wind direction, and precipitation rates; however, ambient temperature may mostly be ignored for short and strict delivery time limits. Furthermore, battery swapping could be highly effective at reducing equipment requirements given worst-case demand.

Given adequate historical data about weather and demand, drone delivery operators should be able to plan efficiently to meet peak demand periods without unacceptable failure rates or excessive costs. Winds will remain an obstacle during some parts of the year unless drone speeds can be improved. Although drones could provide fast delivery times for the vast majority of cases, some failures would be difficult to avoid. Ideally, service areas should remain small enough that travel times are not limited by distance, and overlap of service hubs would provide alternative delivery routes when wind direction is not ideal.

Future research could also examine the likelihood that the delivery of automatic defibrillators would be operable, given that only one-third of OHCA are witnessed by another person. This paper assumed 100% reporting for OHCA events; as such, the rate, μ_n, represents a highest-demand condition, and the time between events would most likely be longer than estimated, as not all would be reported. In the event that someone is able to call emergency services, drone deliveries could be valid

but cannot be employed when another person is not present for operations.

Furthermore, there is an access and equity question associated with a drone's ability to deliver to some areas. For example, airports are often restricted flight zones that do not allow drone operations. Such areas are also areas with higher proportions of lower-income communities. Future research could examine where a delivery system could be employed and what ground delivery systems would be required locally to adjust for access differences. In addition, future research efforts should analyze how COVID-19 and subsequent lockdowns have greatly increased opportunities to deploy fleets of drones for time-sensitive deliveries.

Author Contributions

The authors confirm contribution to the paper as follows: study conception and design: M. Figliozzi, T. Glick; data collection: T. Glick , M. Figliozzi; analysis and interpretation of results: T. Glick, M. Figliozzi, A. Unnikrishnan; draft manuscript preparation: T. Glick, M. Figliozzi, A. Unnikrishnan. All authors reviewed the results and approved the final version of the manuscript.

Declaration of Conflicting Interests

The authors declared no potential conflicts of interest with respect to the research, authorship, and/or publication of this article.

Funding

The authors disclosed receipt of the following financial support for the research, authorship, and/or publication of this article: This research was funded by the Freight Mobility Research Institute, a U.S. Department of Transportation University Transportation Center.

ORCID iDs

Travis B. Glick https://orcid.org/0000-0001-6936-9111
Miguel A. Figliozzi https://orcid.org/0000-0003-2120-4929
Avinash Unnikrishnan https://orcid.org/0000-0001-6737-0485

References

1. Ministry of Infrastructure. *Public Transport Policy and Strategy for Rwanda*. Ministry of Infrastructure, Kigali, 2012.
2. Chen, J. Rwanda has Shown that Healthcare Innovation in the Developing World Means More Than Investing in Technology. *Thomas Reuters Foundation News*, 22 August 2017. https://news.trust.org/item/20170821144058-29rg6/
3. Denby, S. The Super-Fast Logistics of Delivering Blood By Drone. *Wendover Productions*, 2019. https://www.youtube.com/watch?v=bnoUBfLxZz0
4. Scalea, J. R., S. Restaino, M. Scassero, G. Blankenship, S. Bartlett, and N. Wereley.An Initial Investigation of Unmanned Aircraft Systems (UAS) and Real-Time Organ Status Measurement for Transporting Human Organs. *IEEE Journal of Translational Engineering in Health and Medicine*, Vol. 6, 2018, pp. 1–7.
5. Brooks, S. C., R. H. Schmicker, T. D. Rea, T. P. Aufderheide, D. P. Davis, L. J. Morrison, R. Sahni, G. K. Sears, D. E. Griffiths, G. Sopko, S. S. Emerson, P. Dorian and ROC Investigators. Dorian and ROC Investigators. Out-of-Hospital Cardiac Arrest Frequency and Survival: Evidence for Temporal Variability. *Resuscitation: Official Journal of the European Resuscitation Council*, Vol. 81, No. 2, 2010, pp. 175–181.
6. American Heart Association. Heart Disease and Stroke Statistics - 2018 Update: A Report From the American Heart Association. *Circulation*, Vol. 137, No. 12, 2018, pp. e67–e492..
7. HeartSine Samaritan PAD 450P AED. *Foremost*, 2019. https://www.foremostequipment.com/heartsine-samaritan-pad-450p-aed-new/
8. Chan, P. S., H. M. Krumholz, G. Nichol, and B. K. Nallamothu. Delayed Time to Defibrillation after In-Hospital Cardiac Arrest. *The New England Journal of Medicine*, Vol. 358, No. 1, 2008, pp. 9–17.
9. Mell, H. K., S. N. Mumma, B. Heistand, B. G. Carr, T. Holland, and J. Stopyra. Emergency Medical Services Response Times in Rural, Suburban, and Urban Areas. *JAMA Surgery*, Vol. 152, No. 10, 2017, pp. 983–984.
10. Glover, M., and T. Colton. Workhorse Partners with USOG to Launch Pilot Programs for Drone Delivery of Medical Supplies. *BioSpace*, 8 October 2019. https://www.biospace.com/article/releases/workhorse-partners-with-usog-to-launch-pilot-programs-for-drone-delivery-of-medical-supplies/
11. Claesson, A., A. Bäckman, M. Ringh, L. Svensson, P. Nordberg, T. Djärv, and J. Hollenberg. Time to Delivery of an Automated External Defibrillator Using a Drone for Simulated Out-of-Hospital Cardiac Arrests vs Emergency Medical Services. *JAMA*, Vol. 317, No. 22, 2017, pp. 2332–2334.
12. Pulver, A., and R. Wei. Optimizing the Spatial Location of Medical Drones. *Applied Geography*, Vol. 90, 2018, pp. 9–16.
13. Boutilier, J. J., S. C. Brooks, A. Janmohamed, A. Byers, J.E. Buick, C. Zhan, A.P. Schoellig, S. Cheskes, L. J. Morrison, and T. C. Y. Chan. Optimizing a Drone Network to Deliver Automated External Defribrillators. *Applied Geography*, Vol. 135, No. 25, 2017, pp. 2454–2465.
14. Casella, G., and R. L. Berger. *Statistical Inference*, 2nd ed. Daxbury, Pacific Grove, CA, 2002.
15. Nordenskjöld, A. M., K. M. Eggers, T. Jernberg, M. A. Mohammad, D. Erlinge, and B. Lindahl. Circadian Onset and Prognosis of Myocardial Infarction with Non-Obstructive Coronary Arteries (MINOCA). *PLoS One*, Vol. 4, 2019, p. 14.
16. Figliozzi, M. A. Lifecycle Modeling and Assessment of Unmanned Aerial Vehicles (Drones) CO2e Emissions. *Transportation Research Part D*, Vol. 57, 2017, pp. 251–261.
17. Microdrones. The Heavy-Lifting Drone md4-3000. 2019. https://www.microdrones.com/en/drones/md4-3000/.

18. Alibaba. *36v 10ah Lipo Battery*. 2019. https://www.alibaba.com/product-detail/36v-10ah-lipo-battery-for-e_60444386060.html
19. Aniwaa. *MD4-3000 Microdrones*. Aniwaa Pte Ltd, 2019. https://www.aniwaa.com/product/drones/microdrones-md4-3000/
20. Rickert, J. Simulating from the Bivariate Normal Distribution in R. *Revolutions*, 4 August 2016. https://blog.revolutionanalytics.com/2016/08/simulating-form-the-bivariate-normal-distribution-in-r-1.html
21. Normal Distribution. 2019. https://en.wikipedia.org/wiki/Normal_distribution
22. Sum of Normally Distributed Random Variables, 2019. https://en.wikipedia.org/wiki/Sum_of_normally_distributed_random_variables
23. Li, Z., F. Brissette, and J. Chen. Finding the Most Appropriate Precipitation Probability Distribution for Stochastic Weather Generation and Hydrological Modelling in Nordic Watersheds. *Hydrological Processes*, Vol. 27, 2013, pp. 3718–3729.
24. *Gamma Distribution*, 2019. https://en.wikipedia.org/wiki/Gamma_distribution
25. Qin, Z., W. Li, and X. Xionga. Estimating Wind Speed Probability Distribution Using Kernel Density Method. *Electric Power Systems Research*, Vol. 81, No. 12, 2011, pp. 2139–2146.
26. NOAA. *Climate Data Online*, 2019. https://www.ncdc.noaa.gov/cdo-web/
27. Samadani, E. *Modeling of Lithium-ion Battery Performance and Thermal Behavior in Electrified Vehicles*. University of Waterloo, Waterloo, ON, 2015.
28. U.S. Forest Service. *If You Fly, We Can't," United States Department of Agriculture*, 2019. https://www.fs.usda.gov/managing-land/fire/uas/if-you-fly

Opinions given as well as any errors or omissions are the sole responsibility of the authors.